Guided wave propagation along the surface of a one-dimensional solid–fluid phononic crystal

2013 J. Phys. D: Appl. Phys. 46 365305

(http://iopscience.iop.org/0022-3727/46/36/365305)

IOP PUBLISHING JOURNAL OF PHYSICS D: APPLIED PHYSICS

J. Phys. D: Appl. Phys. **46** (2013) 365305 (9pp) doi:10.1088/0022-3727/46/36/365305

Guided wave propagation along the surface of a one-dimensional solid–fluid phononic crystal

Rayisa P Moiseyenko[1,2,3], Nico F Declercq[2] and Vincent Laude[1]

[1] Institut FEMTO-ST, Universitè de Franche-Comtè and CNRS, 32 avenue de l'Observatoire, F-25044 Besançon Cedex, France

[2] Georgia Institute of Technology, UMI Georgia Tech–CNRS, George W. Woodruff School of Mechanical Engineering, Georgia Tech Lorraine, 2 rue Marconi, 57070 Metz-Technopole, France

E-mail: rayisa.moiseyenko@gmail.com

Received 15 May 2013, in final form 9 July 2013
Published 22 August 2013
Online at stacks.iop.org/JPhysD/46/365305

Abstract

We consider an arbitrary periodic corrugated surface of a semi-infinite elastic solid that is immersed in a fluid, forming a one-dimensional phononic crystal. We study the existence and the polarization of guided waves that propagate along the interface. A coupled elastic-acoustic variational model is devised to obtain the dispersion of guided waves, which is implemented with a finite element method. It is found that the deeply corrugated interface supports a family of interface waves whose phase velocity decreases as the corrugation depth increases. Among these interface waves, some display an evanescent decay in the fluid that is reminiscent of the Scholte–Stoneley wave, while others propagate in the solid without causing significant pressure variation in the fluid, or cause localized pressure variations only inside the corrugation openings. The obtained results open the way for the study of conversions between bulk and surface waves in solid–fluid phononic crystals, and their use for wave confinement at the surface.

(Some figures may appear in colour only in the online journal)

1. Introduction

Phononic crystals are periodic structures consisting of at least two different materials which are often considered with regards to their property of creating complete band gaps, or frequency ranges where wave propagation through crystal is forbidden for any angle of incidence [1]. For solid–solid phononic crystals, or phononic crystals of holes in solids, elastic wave propagation is generally considered to be undisturbed by the atmosphere that surrounds the crystal, which is treated as if it were a vacuum. In the case of sonic crystals, for which the surrounding medium is composed of air, transduction of elastic waves into rigid solid parts can also generally be ignored. There are certain sonic crystals, however, for which this transduction must be taken into account, such as with foams hosting multiple local resonances [2]. The case of phononic crystals immersed in water, furthermore, calls for adequate models of wave propagation including fluid–structure interaction, as the interplay of acoustic waves in the fluid and elastic waves in the solid must be explicitly accounted for. Phononic crystal plates immersed in water have received strong attention recently, in connection with the phenomenon of enhanced acoustic transmission (EAT) [3–5]. It was shown that they can support the propagation of surface waves that are confined to the plate–fluid interface [6, 7]. Surface waves propagating at the planar interface of a solid medium and a fluid are termed Scholte–Stoneley waves (SSWs) [8, 9]. This appellation is generally also used when the interface presents a shallow corrugation [10]. In addition, Estrada *et al* [7] considered solid–solid phononic crystal plates without a geometric corrugation but a periodic variation of the material constants, for which they could obtain experimentally the SSW dispersion by attaching a small piezoelectric patch transducer directly to the plate. The use of such a transduction method originates from the fact that SSWs on flat surfaces cannot be excited experimentally by plane waves originating from

[3] Present address: Institut d'Electronique de Microèlectronique et de Nanotechnologie, Citè Scientifique, 59652 Villeneuve d'Ascq Cedex, France.

acoustic transducers placed in the surrounding water. This is because the required matching of wavevectors projected along the interface cannot be satisfied, as the SSW velocity is smaller than the fluid velocity. Experimental excitation of SSWs on planar interfaces by means of the laser-induced thermoelastic effect was reported by Desmet *et al* [11]. In these experiments, the velocity of SSWs excited thermoelastically on mercury/plexiglas or mercury/fused silica plane interfaces and detected by the technique of light beam deflection agreed well with theoretical predictions. Glorieux *et al* [12, 13] further illustrated that leaky Rayleigh and SSW laser-ultrasonic spectroscopy or impulsive stimulated thermal scattering is a suitable technique for the characterization of soft solids and coated solids down to the micron scale. SSWs can alternatively be generated through diffraction of plane waves by a corrugated interface, as periodicity can provide an additional reciprocal lattice wavevector to satisfy the matching of wavevectors projected along the interface. In this context, SSWs were proposed as the reason for the backward beam displacement on shallow one-dimensional corrugated brass grating [10, 14, 15].

From the above discussion, it is clear that there is a need for models of wave dispersion along arbitrary solid–fluid periodic interfaces. In this work, we specifically consider guided wave propagation along a deeply corrugated solid–fluid interface that defines a one-dimensional phononic crystal. We are not aware of any analytical model for obtaining the dispersion of interface waves in this case, contrary to the planar case. Estrada *et al* [7] obtained the dispersion of a phononic crystal plate immersed in water by coupling a plane wave expansion method in the solid with a Green's function solution for the semi-infinite fluid medium. The particular arrangement was a periodic variation of the elastic properties of the solid–solid plate, in the absence of a corrugation of the surface. Because of the difficulties of the plane wave expansion method to handle fluid–solid compositions properly [16], the method can hardly be extended to the case of corrugated plates. In order to build a solution for the general corrugation problem, we devise a variational formulation of coupled elastic (in the solid) and acoustic (in the fluid) wave propagation. A finite element method implementing the variational formulation is then used for numerical simulations. Model validation is achieved by comparing the computed dispersion diagrams with Brekhovskih's solution for a flat interface [17]. Dispersion diagrams for deeply corrugated silicon plates immersed in water are then presented. They show the appearance of a family of interface waves whose properties as a function of the corrugation depth are discussed.

2. Theory

The planar interface and the 1D corrugated interface, or phononic crystal grating [18, 19], separating solid and fluid domains are depicted in figure 1. We first consider the planar interface whose unit-cell is shown in figure 1(*a*). Although we wish to model the propagation of waves at the interface between two semi-infinite media, we consider finite heights for both the fluid and the solid. In doing so, we assume that the

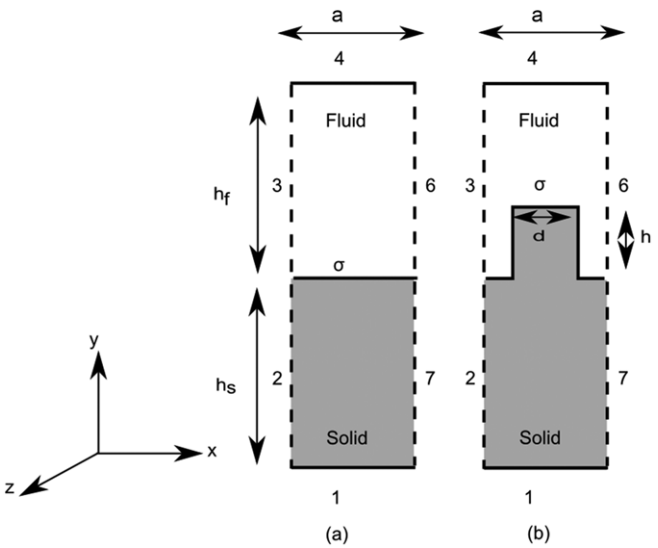

Figure 1. Two-dimensional unit-cells used in finite element simulations of (*a*) a plane solid/fluid interface and (*b*) a 1D corrugated solid/fluid interface. The corrugation period is a. The groove height is h and its width is d. The numbers indicate the different borders used for mesh generation and for applying boundary conditions. Periodic boundary conditions are imposed on the pair of boundaries 2 and 7, and 3 and 6. Acoustic-elastic coupling is implemented on boundary σ separating the fluid and the solid domains. Boundaries 1 and 4 are left free.

wave decays exponentially sufficiently fast from both sides of the interface. As we discuss later, this is generally true for the part of the dispersion diagram that lies under the sound cone, and some discrepancies can result in small wavenumbers. In our computations, the heights h_f for the fluid domain and h_s for the solid domain are taken to be equal to $15a$, with a the corrugation period.

For the planar interface, we consider wave propagation in the z direction and we plot dispersion diagrams given the angular frequency ω as a function of the z component of the wavevector, k_z. A direct comparison can be performed with Brekhovskih's formula in this case. Indeed, Brekhovskhih deduces the SSW dispersion relation from the acousto-elastic equations with assumption of absence of tangential stress, continuity of pressure and normal stress, and continuity of normal displacements at the interface. The dispersion relation is given in implicit form as a real root s of

$$4\sqrt{1-s}\sqrt{1-qs} - (s-2)^2 = (\rho s^2)\sqrt{1-sq}/\sqrt{1-sr}, \tag{1}$$

where

$$\rho = \rho_f/\rho_s, \tag{2}$$

$$q = (c_s/c_l)^2, \tag{3}$$

$$r = (c_s/c_f)^2, \tag{4}$$

$$s = (c_{ss}/c_s)^2. \tag{5}$$

In these expressions, ρ_f and ρ_s are the mass densities of the fluid and of the solid, c_s and c_l are the shear and longitudinal sound velocities in the solid, c_f is the sound velocity in the fluid and c_{ss} is the velocity of the SSW. The wavenumber

thus enters implicitly via the dispersion relation $k_z = \omega/c_{ss}$ and correspondence with our model can only be expected in the large wavenumber limit. The roots of Scholte–Stoneley equation were studied in detail by Pilant [20], Ansell [21], and Padilla [22] for a planar interface between a solid and a fluid in the case $c_{ss} < c_s < c_f < c_l$. The SSW is given by a real root and the leaky Rayleigh wave can in principle be identified from the complex roots. The leaky Rayleigh wave propagates with a phase velocity slightly lower than c_s and radiates energy into the fluid. In contrast, the SSW propagates along the boundary with a phase velocity less than all bulk velocities in the fluid and in the solid. Its energy and particle displacement are localized mostly in the fluid, and to a lesser extent in the solid [23].

The unit-cell geometry for the corrugated plate is presented in figure 1(*b*). In this case, propagation is considered along the x-axis, and we plot dispersion diagrams given the angular frequency ω as a function of the x component of the wavevector, k_x. Periodic boundary conditions are imposed on boundary pairs: for pressure on boundaries 3 and 6, and for displacements on boundaries 2 and 7. In addition, boundaries 1 and 4 are left free (Neumann boundary condition), as in the planar interface case.

For both the planar and the corrugated interface case, acoustic–elastic wave coupling is achieved by boundary conditions applied on boundary σ. First, at interface σ the normal acceleration is continuous across both domains and is related to the normal derivative of the pressure p in the fluid,

$$\rho_f \omega^2 u_n = \frac{\partial p}{\partial n}, \tag{6}$$

with u_n the normal component of the displacement and ρ_f the mass density of the fluid. Second, the normal traction must be continuous across the interface, i.e.

$$T_{ij} n_j = -p n_i, \tag{7}$$

with T_{ij} the stress tensor inside the solid. The minus sign accounts for the difference in definition of the normal unit vector $\boldsymbol{n}$ as seen from within the fluid or the solid; the normal is orthogonal to boundary σ and points outwards of the considered domain.

As detailed in the appendix, a variational formulation of the acoustic–elastic coupling problem can be obtained from the above boundary conditions. When expressed numerically using the finite element method, it leads to a generalized eigenvalue problem of the form

$$A(k)\boldsymbol{x} = \omega^2 B\boldsymbol{x}. \tag{8}$$

The vector $\boldsymbol{x}$ is composed of the values of pressure in the fluid and displacements in the solid at the nodes of the mesh of the unit-cell. Matrices $A(k)$ and B contain non-diagonal terms that account for the coupling of acoustic and elastic waves. Solving the eigenvalue problem (8) as a function of the wavevector k, dispersion diagrams are readily obtained as $\omega(k)$. The eigenvectors $\boldsymbol{x}$ further give the modal shape of each solution.

3. Results

3.1. Smooth interface

We first consider the planar interface between a fluid and a solid, according to the unit-cell depicted in figure 1(*a*). Three different combinations of materials are considered: mercury/plexiglas, water/PVC, and water/silicon. The velocities of bulk acoustic and elastic waves for these materials are given in table 1. Two different cases can be distinguished. First, for the couples mercury/plexiglas and water/PVC, the shear velocity is smaller than the sound velocity in water. As a result, there is a significant difference between c_f and c_{ss}, and the SSW velocity can be easily extracted from experiment. Experimental measurements are available for mercury/plexiglas [12, 13] and water/PVC [22]. Second, for the couple water/silicon, the shear velocity is larger than the sound velocity in water. When this is the case, it is usually found that c_{ss} is close to c_f and their experimental separation is somewhat more difficult. Silicon is considered here because it is the most common material found in MEMS technologies, but similar results would hold with, e.g. brass [10].

The radiative region, or sound cone, is depicted in grey in the simulated dispersion diagrams presented in figure 2. It is limited by the sound line, whose slope is given by the smallest of c_s and c_f (since $c_s < c_l$ for any solid material). The dispersion diagrams are obtained numerically considering a finite thickness for both fluid and solid. The dispersion curves are then rigorously those of waves propagating inside a composite fluid–solid plate. Outside the sound cone, however, these waves are evanescent both in the fluid and in the solid. The dispersion curve of any wave propagating along the interface must then appear outside the sound cone. In the long wavenumber limit, in addition, the SSW must appear as the asymptotic limit of some dispersion curve [24]. When the product of frequency times plate thickness $\omega h_s/2\pi$ is small, waves outside the sound cone are only weakly evanescent and their velocity is influenced by the surfaces terminating the computational domain. As a result, the bands that eventually converge to the SSW as the frequency increases first emerge as flexural waves at low frequencies. This is not a limitation in practice, since the convergence rate can be made faster by simply increasing the plate thickness.

The cases of mercury/plexiglas in figure 2(*a*) and of water/PVC in figure 2(*b*) correspond to $c_s < c_f < c_l$, i.e. the acoustic velocity in the fluid is in between the shear and the longitudinal elastic velocities in the solid. Under this setting, and with the condition of zero surface traction considered numerically for boundary 1, the Rayleigh surface wave at the free solid surface appears in the non-radiative region, together with the SSW. The Rayleigh wave velocity is easily found from the dispersion relation (1) by setting $\rho = 0$, i.e. the Scholte–Stoneley dispersion relation resolves in the Rayleigh dispersion relation when the fluid density vanishes. This particular band is spurious for the problem we are considering and should be disregarded in the analysis. In the case of water/silicon in figure 2(*c*), $c_f < c_s < c_l$, the Rayleigh wave appears inside the sound cone and thus only the SSW is expected in the non-radiative region. In summary,

Table 1. Scholte–Stoneley velocity, c_{ss}, as obtained from Brekhovskih's dispersion relation [17] and by the FEM method for a planar interface. The FEM value is given by the asymptotic limit of ω/k for the lowest band, as the wavenumber k goes to infinity, with ω the angular frequency.

Material	c_{ss} ($m\,s^{-1}$)	FEM c_{ss} ($m\,s^{-1}$)	c_f ($m\,s^{-1}$)	c_s ($m\,s^{-1}$)	c_l ($m\,s^{-1}$)	ρ_f ($kg\,m^{-3}$)	ρ_s ($kg\,m^{-3}$)
Mercury/plexiglas	448	448	1450	1300	2750	13500	1190
Water/PVC	914	914	1485	1112	2236	1000	1560
Water/silicon	1484	1484	1485	5800	8400	1000	2330

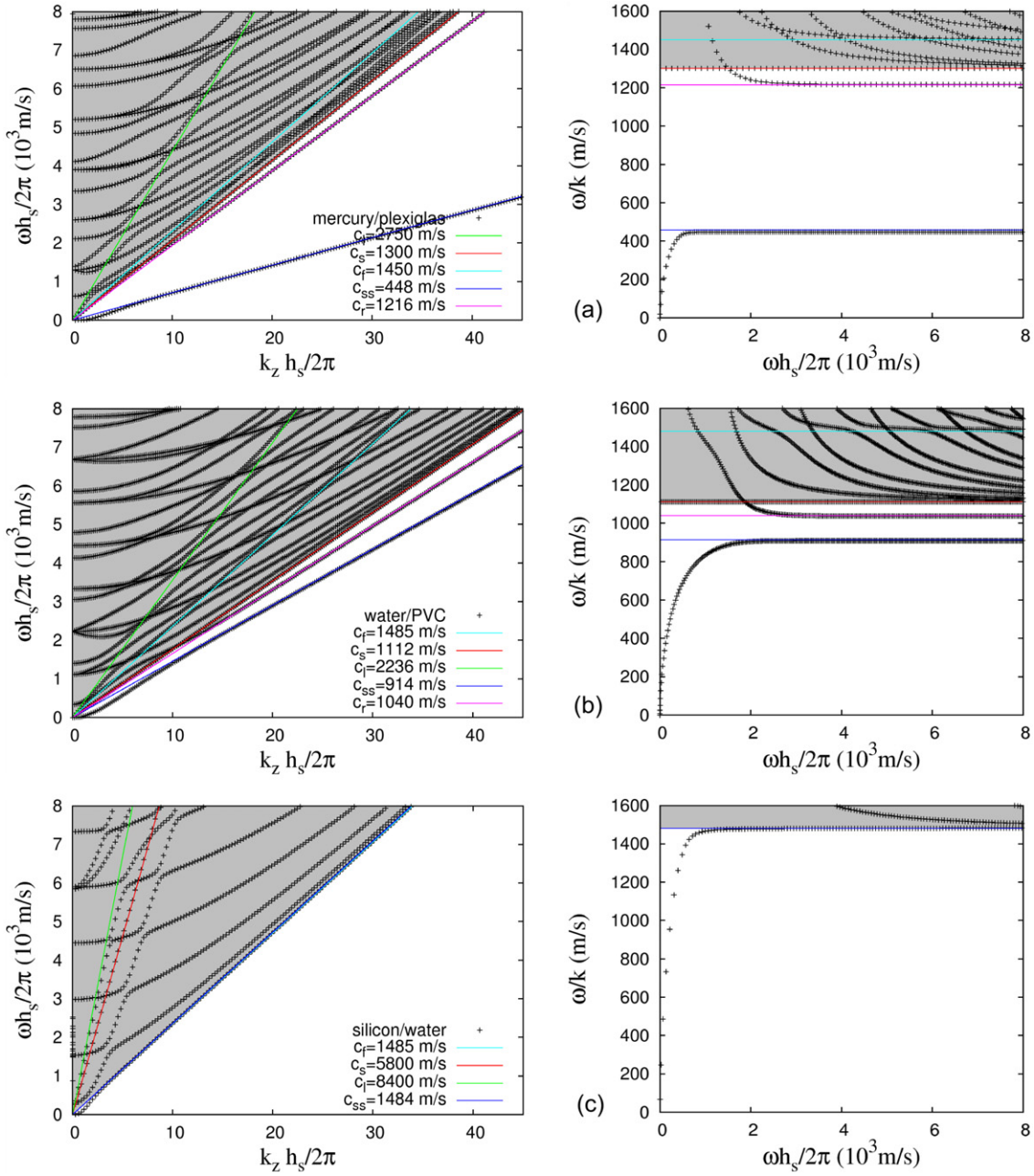

Figure 2. Dispersion relation for acoustic–elastic waves guided along the planar interface between a solid and a fluid. The band structure—or the $\omega(k_z)$ dispersion relation—is shown left and the phase velocity ω/k_z is shown right as a function of frequency. h_s is the solid thickness. The cases of (*a*) mercury–plexiglass, (*b*) water–PVC and (*c*) water–silicon are presented.

for the three cases considered in figure 2, there are only one or two dispersion bands appearing under the sound cone, in accordance with the discussion above. As k goes to infinity, the phase velocity ω/k of these bands approaches asymptotic limit corresponding to the SSW or to the Rayleigh wave, when the latter is present. The agreement between the SSW velocity evaluated by FEM and according to Brekhovskih's method [17] is excellent, as table 1 summarizes.

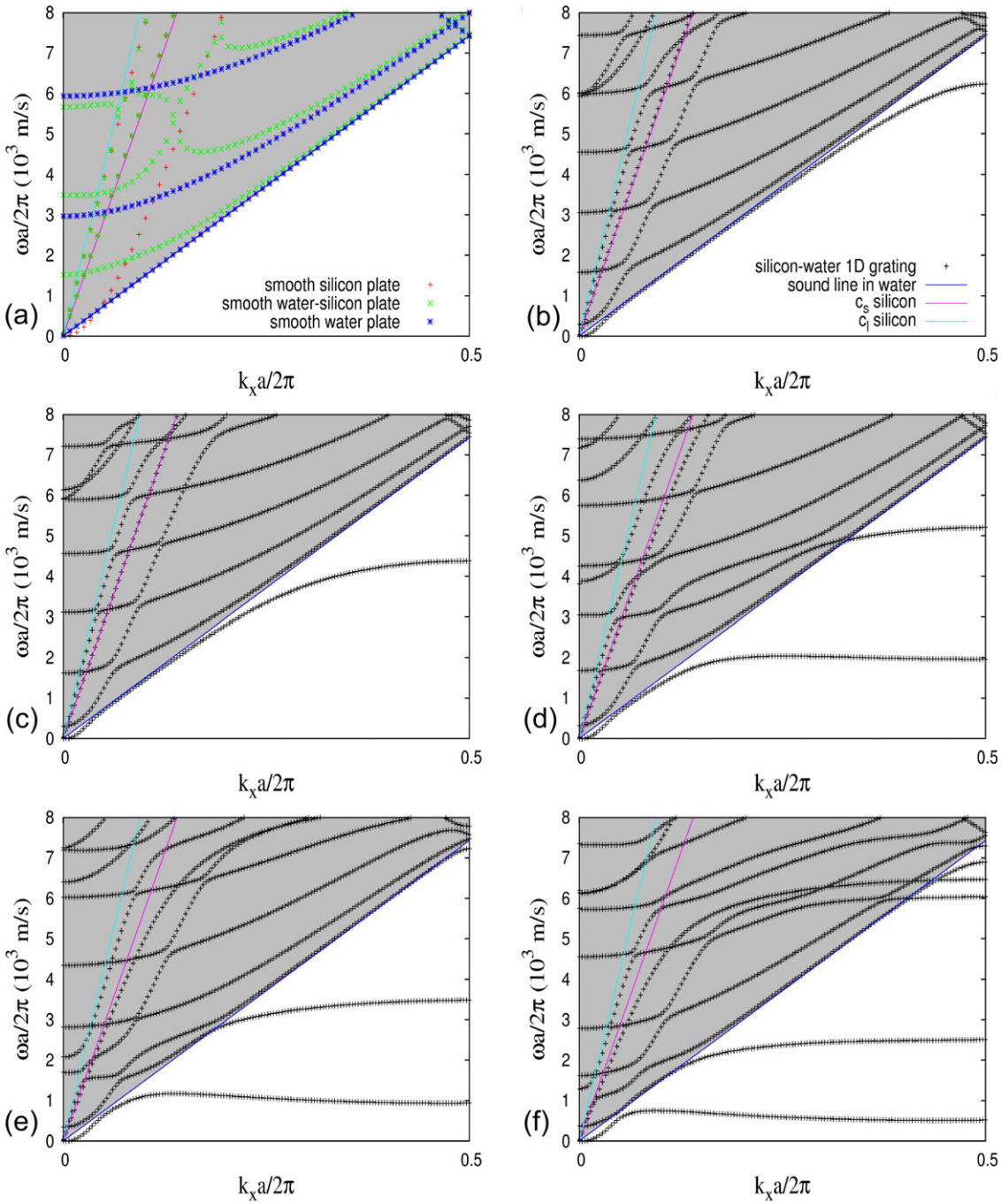

Figure 3. Band structures $\omega(k_x)$ for guided waves obtained by FEM for a corrugated interface of rectangular profile with normalized corrugation depth (*a*) $h/a = 0$, (*b*) 0.25, (*c*) 0.5, (*d*) 1, (*e*) 1.5 and (*f*) 2. a is the corrugation pitch. The example is given for a corrugated silicon plate immersed in water. In the case of the planar interface (*a*), the band structures for a free silicon plate and and free water plate are also shown for comparison.

3.2. Corrugated interface

We now turn to the corrugated solid–fluid interface situation and consider for numerical experiments the interface between silicon and water. This choice of materials is justified from the availability of MEMS technologies for etching deep corrugations in silicon wafers. The general trends that we describe below, however, are expected to remain valid for other material combinations. The computational unit-cell is of the form displayed in figure 1(*b*), with a the grating period, d the corrugation width, and h the corrugation depth. For definiteness, $d/a = 0.5$ is chosen and h/a is varied.

Figure 3 shows dispersion diagrams for six different values of h/a, ranging from 0 to 2.0. The interesting part of these diagrams is the non-radiative region appearing below the sound line in water. It can be seen that increasing the corrugation depth results in two main phenomena. First, new bands appear in the non-radiative region as the corrugation depth is increased, corresponding to the existence of more and more interface waves, in contrast to the existence of only the SSW

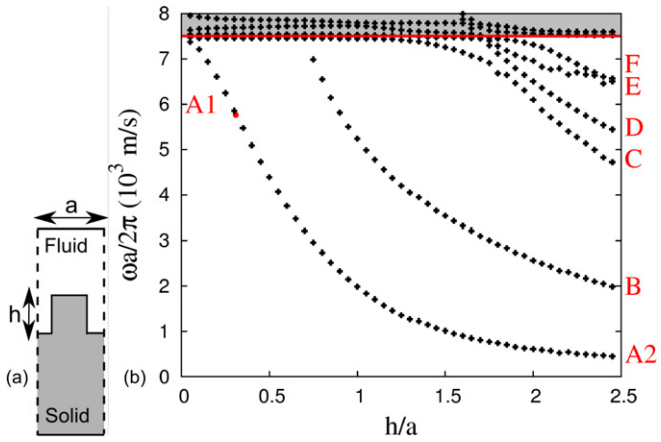

Figure 4. (*a*) Sketch of the corrugated silicon plate immersed in water. (*b*) Evolution of bands in the non-radiative zone, i.e. for guided waves at the interface, for $k_x a/2\pi = 0.5$, when the normalized corrugation depth h/a is varied from 0 to 2.5. a is the corrugation pitch.

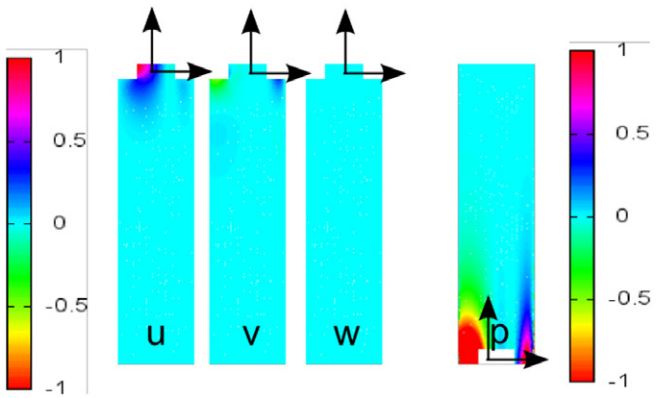

Figure 5. Normalized displacements and pressure for eigenmode A1 in figure 4. The corrugation depth $h/a = 0.25$. Normalization is performed so that the maximum total displacement is 1 nm; pressure is correspondingly in units of 10^8 Pa.

for the planar interface. We discuss later the polarization of these interface waves, but we already observe that the situation is reminiscent of the case of a deeply corrugated semi-infinite solid in a vacuum [25–27]. Second, the bands in the non-radiative region become flatter as the depth increases, indicating that the group velocity, $v_g = \partial\omega/\partial k$, becomes very small. For the lowest band and starting from $h/a = 1$, the group velocity is even slightly negative for intermediate values of $k_x a/(2\pi)$.

Figure 4 presents the evolution of the reduced frequency $\omega a/(2\pi)$ at resonance, i.e. for $k_x a/(2\pi) = 0.5$, as a function of the normalized corrugation depth h/a. A total of six different interface waves can be identified in the non-radiative region when h/a increases from 0 to 2.5. Obviously, more and more interface waves would appear for even higher corrugation depths.

Even though each interface wave clearly lies on a distinct dispersion curve, the detailed polarization field can undergo strong transformations as the corrugation depth increases. As an illustration, interface wave A1 depicted in figure 5 for $h/a = 0.25$ is of the Scholte–Stoneley type, with coupled displacements in the sagittal plane and an evanescent pressure field extending far into water. Interface wave A2 on the same dispersion curve but for $h/a = 2.5$, is a strongly evanescent quasi-longitudinal surface wave giving rise to almost no pressure variation in water, as figure 6(*a*) shows. Interface wave B and C illustrated in figures 6(*b*) and (*c*) have coupled displacements in the sagittal plane and create a pressure variation that is confined inside the corrugation. Interface wave F in figure 6(*f*) is also of a similar type, with the pressure field extending deeply in open water. They could be interesting resonant modes for sensing applications. Indeed, the acoustic energy is localized at the interface and its amplitude is enhanced as compared to the case of bulk acoustic waves. Then if analytes were placed in the fluid inside the trenches, they would be able to interact strongly with the wave guided at the interface. It would also be possible to use the solid plate for both generation and detection purposes, by having the circuitry on the plate. Interface wave D displayed in figure 6(*d*) is a pure shear horizontal wave that induces no pressure variation in water. Such a wave can clearly only be excited from the solid. Interface wave E is mostly vertically shear polarized inside the solid ridges and is accompanied with an evanescent pressure field extending well into open water. The extension of the pressure field in open water for the different interface waves depends directly on the distance from the dispersion curve to the sound line, as suggested by the square-root dependence in the dispersion relation for the SSW (1).

From the different observations made above, it is clear that the corrugation depth should never be neglected when designing corrugated plates for the generation of waves at the interface of a solid and a fluid. Furthermore, the SSW characteristics—obtained for a planar interface—are lost rapidly as the corrugation depth is increased. Conversely, the existence of several families of interface waves for deep corrugations opens the way for experiments where they could be generated either from the fluid, by diffraction of bulk acoustic waves on the grating itself [10], or from the solid, using either a transducer of elastic waves attached directly to the solid plate [7] or laser ultrasound generation as in the case of planar interfaces [11–13].

4. Conclusion

This work has been devoted to a study of guided acoustic–elastic waves propagating at the planar or corrugated interface between a fluid and a solid, including the SSW and its transformations as the corrugation depth is made deeper. We stress that guided waves propagate along the interface with a phase velocity less than both bulk velocities in the fluid and in the solid. We specifically proposed a variational form of the coupled acoustic–elastic problem that is valid for an arbitrary solid and corrugation profile, though we restricted numerical examples to the rectangular sawtooth profile. The variational form is easily amenable to finite element implementation. The value of the exact SSW velocity predicted by Brekhovskih's formula is recovered as an asymptotic long-wavelength limit. For deep corrugations, a family of interface waves is found

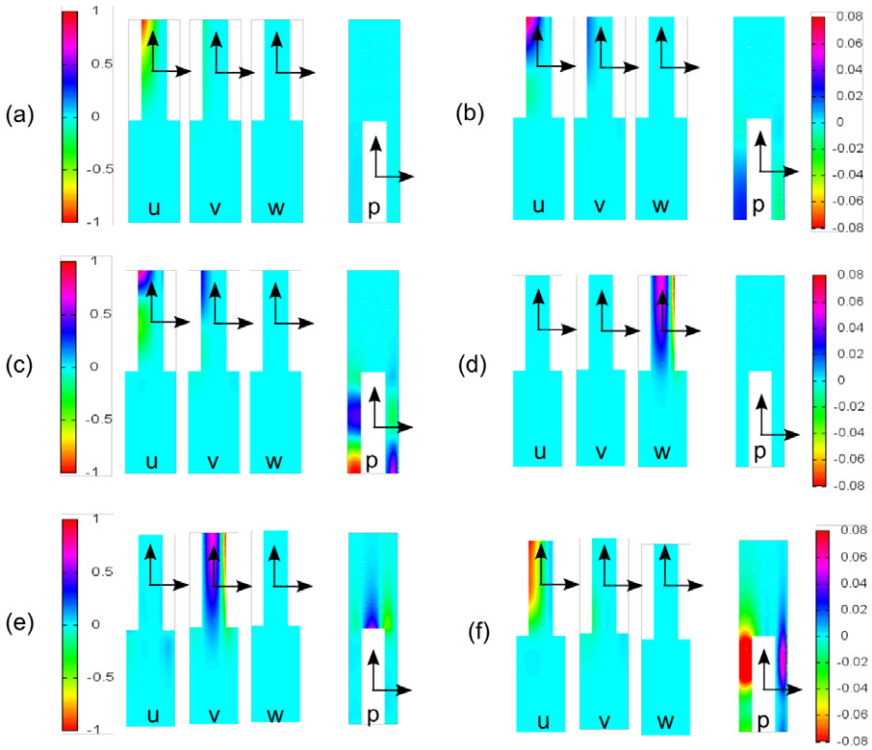

Figure 6. Normalized displacements and pressure for eigenmodes A2, B, C, D, E and F in figure 4. The corrugation depth $h/a = 2.5$. Normalization is performed so that the maximum total displacement is 1 nm; pressure is correspondingly in units of 10^8 Pa.

whose phase velocity decreases as the corrugation depth increases. Among these interface waves, some display an evanescent decay in the fluid that resembles that of the SSW, but others propagate in the solid without causing significant pressure variation, or cause localized pressure variations only in the fluid inside the corrugation openings. The band structures reveal slow interface modes that could in principle be excited using plane wave diffraction, laser ultrasonics, or piezoelectric transducers attached to the solid. The model was implemented in the two-dimensional case of corrugation gratings, but it can be straightforwardly extended to the three-dimensional analysis of phononic crystals of holes or pillars immersed in a fluid such as water.

Acknowledgments

Financial support by the Agence Nationale de la Recherche under grant ANR-09-BLANC-0167-01 is gratefully acknowledged. VL acknowledges the support of the Labex ACTION program (contract ANR-11-LABX-01-01).

Appendix. Variational formulation of elastic-acoustic interaction and finite element implementation

Following the procedure given in [28] for acoustic waves in phononic crystals, a variational formulation of elastic-acoustic interaction is proposed in this appendix.

We consider time-harmonic waves with angular frequency ω. The scalar equation of motion for acoustic waves in the fluid can then be written for the pressure only as [29, 30]

$$\frac{\omega^2}{B} p + \nabla \cdot \left(\frac{1}{\rho_\mathrm{f}} \nabla p \right) = 0, \tag{A.1}$$

with ρ_f the mass density of the fluid and B its adiabatic compressibility for zero heat conduction (implying that we neglect thermal phenomena in the model). Motion in solid is described by Hooke's law

$$T_{ij} = c_{ijkl} \frac{\partial u_k}{\partial x_l}, \tag{A.2}$$

and by Newton's second law

$$\omega^2 \rho_\mathrm{s} u_i + T_{ij,j} = 0. \tag{A.3}$$

Here, c is the rigidity tensor of rank 4 and ρ_s is the mass density of the solid.

A variational formulation can be derived using the basic equations (A.1)–(A.3), and the coupling boundary conditions (6), (7) at the fluid–solid interface. We multiply (A.1) by test function q living in the same finite element space as p and (A.3) by test function ψ_i $(i = 1, 2, 3)$ living in the same finite element space as u_i, and integrate over the fluid and the solid domains. The terms containing a divergence are transformed by applying Green's formula and incorporating coupling boundary conditions at the fluid–solid interface, according to

$$\int_{\Omega_\mathrm{f}} \nabla . \left(\frac{1}{\rho_\mathrm{f}} \nabla p \right) q \mathrm{d}r = \omega^2 \int_\sigma q u_\mathrm{n} \mathrm{d}n - \int_{\Omega_\mathrm{f}} \nabla q \left(\frac{1}{\rho_\mathrm{f}} \nabla p \right) \mathrm{d}r \tag{A.4}$$

and

$$\int_{\Omega_s} T_{ij,j}\psi_i \mathrm{d}r = -\int_{\sigma} p\psi_n \mathrm{d}n - \int_{\Omega_s} \psi_{i,j} T_{ij} \mathrm{d}r, \qquad (A.5)$$

with $u_n = u_i n_i$ and $\psi_n = \psi_i n_i$. In the last two expressions, it should be noted that the fluid–solid boundary σ is oriented differently, since the unit normal n_i is exterior to domain Ω_f in (A.4) but exterior to domain Ω_s in (A.5). Upon rearranging terms, a variational formulation unifying elements in space and on the boundary is obtained as

$$\omega^2 \left(\int_{\Omega_f} q \frac{1}{B} p \mathrm{d}r + \int_{\sigma} q u_n \mathrm{d}n \right) = \int_{\Omega_f} q_{,i} \frac{1}{\rho_f} p_{,i} \mathrm{d}r, \qquad (A.6)$$

$$\omega^2 \int_{\Omega_s} \psi_i \rho_s u_i \mathrm{d}r = \int_{\sigma} p\psi_n \mathrm{d}n + \int_{\Omega_s} \psi_{i,j} c_{ijkl} u_{k,l} \mathrm{d}r, \qquad (A.7)$$

The inclusion of the wavevector dependence follows the application of the Bloch–Floquet theorem. Specifically, it is sufficient [28] to make the following replacements in the pair of equations above:

$$p_{,i} = \overline{p}_{,i} - \jmath k_i \overline{p}, \qquad q_{,i} = \overline{q}_{,i} + \jmath k_i \overline{q}, \qquad (A.8)$$

$$u_{k,l} = \overline{u}_{k,l} - \jmath k_l \overline{u}_k, \quad \psi_{i,j} = \overline{\psi}_{i,j} + \jmath k_j \overline{\psi}_i. \qquad (A.9)$$

Finally, the pair of equations (A.6), (A.7) can be cast in the form of a generalized eigenvalue problem $\omega(k)$

$$A(k)\boldsymbol{x} = \omega^2 B \boldsymbol{x}. \qquad (A.10)$$

where vector $\boldsymbol{x}$ is composed of the values of p and $u_i, i = 1, 2, 3$ at the nodes of the meshes of the domains Ω_f and Ω_s, respectively. The block matrices $A(k)$ and B can be decomposed as

$$A(k) = \begin{bmatrix} A_{11}(k) & 0 \\ A_{21} & A_{22}(k) \end{bmatrix}, \qquad (A.11)$$

$$B = \begin{bmatrix} B_{11} & B_{12} \\ 0 & B_{22} \end{bmatrix}. \qquad (A.12)$$

The square block matrices $A_{11}(k)$ and B_{11} ($A_{22}(k)$ and B_{22}, respectively) define the uncoupled acoustic (elastic, resp.) problem. The rectangular block matrices A_{21} and B_{12} are the coupling terms of the equation, as the acoustic and elastic problems would be uncoupled if they were to vanish. Coupling occurs solely from the boundary conditions (6,7). In practice, the variational formulation above and its numerical solution were coded with FreeFem++ [31] for all examples shown.

References

[1] Kushwaha M S, Halevi P, Dobrzynski L and Djafari-Rouhani B 1993 Acoustic band structure of periodic elastic composites *Phys. Rev. Lett.* **71** 2022–5

[2] Romero-García V, Krynkin A, Garcia-Raffi L M, Umnova O and Sańchez-Pérez J V 2013 Multi-resonant scatterers in sonic crystals: Locally multi-resonant acoustic metamaterial *J. Sound Vib.* **332** 184–98

[3] Christensen J, Fernandez-Dominguez A I, de Leon-Perez F, Martin-Moreno L and Garcia-Vidal F J 2007 Collimation of sound assisted by acoustic surface waves *Nature Phys.* **3** 851

[4] Christensen J, Martin-Moreno L and Garcia-Vidal F J 2008 Theory of resonant acoustic transmission through subwavelength apertures *Phys. Rev. Lett.* **101** 014301

[5] Estrada H, Candelas P, Uris A, Belmar F, García de Abajo F J and Meseguer F 2008 Extraordinary sound screening in perforated plates *Phys. Rev. Lett.* **101** 084302

[6] Every A G, Vines R E and Wolfe J P 1999 Line-focus probe excitation of Scholte acoustic waves at the liquid-loaded surfaces of periodic structures *Phys. Rev.* B **60** 11755–60

[7] Estrada H, Candelas P, Belmar F, Uris A, García de Abajo F J and Meseguer F 2012 Engineering surface waves in flat phononic plates *Phys. Rev.* B **85** 174301

[8] Gogoladze V G 1948 Rayleigh waves on the interface between a compressible fluid medium and a solid elastic half-space *Trudy Seismolog. Inst. Acad. Nauk SSSR* **127** 27–32

[9] Scholte J G 1949 On true and pseudo Rayleigh waves *Nederl. Akad. Wetensch., Proc.* **52** 652–3

[10] Breazeale M A and Torbett M A 1976 Backward displacement of waves reflected from an interface having superimposed periodicity *Appl. Phys. Lett.* **29** 456–8

[11] Desmet C, Gusev V, Lauriks W, Glorieux C and Thoen J 1996 Laser-induced thermoelastic excitation of Scholte waves *Appl. Phys. Lett.* **68** 2939–41

[12] Glorieux C, Van de Rostyne K, Nelson K, Gao W, Lauriks W and Thoen J 2001 On the character of acoustic waves at the interface between hard and soft solids and liquids *J. Acoust. Soc. Am.* **110** 1299–306

[13] Glorieux C, Van de Rostyne K, Goossens J, Shkerdin G, Lauriks W and Nelson K A 2006 Shear properties of glycerol by interface wave laser ultrasonics *J. Appl. Phys.* **99** 013511

[14] Teklu A, Breazeale M A, Declercq N F, Hasse R D and McPherson M S 2005 Backward displacement of ultrasonic waves reflected from a periodically corrugated interface *J. Appl. Phys.* **97** 084904

[15] Herbison S W, Vander Weide J M and Declercq N F 2010 Observation of ultrasonic backward beam displacement in transmission through a solid having superimposed periodicity *Appl. Phys. Lett.* **97** 041908

[16] Hou Z, Fu X and Liu Y 2006 Singularity of the Bloch theorem in the fluid/solid phononic crystal *Phys. Rev.* B **73** 024304

[17] Brekhovskikh L M 1980 *Waves in Layered Media* (New York: Academic)

[18] Moiseyenko R P, Herbison S, Declercq N F and Laude V 2012 Phononic crystal diffraction gratings *J. Appl. Phys.* **111** 034907

[19] Moiseyenko R P, Liu J, Declercq N F and Laude V 2013 Blazed phononic crystal grating *Appl. Phys. Lett.* **102** 034108

[20] Pilant W L 1972 Complex roots of the Stoneley-wave equation *Bull. Seismol. Soc. Am.* **62** 285–99

[21] Ansell J H 1972 The roots of the Stoneley wave equation for liquid–solid interfaces *Pure Appl. Geophys.* **94** 172–88

[22] Padilla F, de Billy M and Quentin G 1999 Theoretical and experimental studies of surface waves on solid–fluid interfaces when the value of the fluid sound velocity is located between the shear and the longitudinal ones in the solid *J. Acoust. Soc. Am.* **106** 666–73

[23] Meegan G D, Hamilton M F Il'inskii Yu A and Zabolotskaya E A 1999 Nonlinear Stoneley and Scholte waves *J. Acoust. Soc. Am.* **106** 1712–23

[24] Laude V, Assouar B M and Hou Z 2010 Computation of plate wave dispersion diagrams and surface wave velocities without explicit boundary conditions *IEEE Trans. Ultrason. Ferroelectr. Freq. Control* **57** 1649–54

[25] Laude V, Khelif A, Pastureaud Th and Ballandras S 2001 Generally polarized acoustic waves trapped by high aspect ratio electrode gratings on piezoelectric substrates *J. Appl. Phys.* **90** 2492–7

[26] Laude V, Robert L, Daniau W, Khelif A and Ballandras S 2006 Surface acoustic wave trapping in a periodic array of mechanical resonators *Appl. Phys. Lett.* **89** 083515

[27] Dühring M B, Laude V and Khelif A 2009 Energy storage and dispersion of surface acoustic waves trapped in a periodic array of mechanical resonators *J. Appl. Phys.* **105** 093504

[28] Laude V, Moiseyenko R P, Benchabane S and Declercq N F 2011 Bloch wave deafness and modal conversion at a phononic crystal boundary *AIP Adv.* **1** 041402

[29] Landau L D and Lifshitz E M 1987 *Fluid Mechanics* (Oxford: Pergamon)

[30] Royer D and Dieulesaint E 1999 *Elastic Waves in Solids* (New York: Wiley)

[31] Hecht F 2012 Freefem++ manual, version 3.20